Fabrication of a Macroporous Microwell Array for Surface-Enhanced Raman Scattering

By *Martina Zamuner, David Talaga, Frédérique Deiss, Valérie Guieu, Alexander Kuhn, Paolo Ugo,** and *Neso Sojic**

Here, a colloidal templating procedure for generating high-density arrays of gold macroporous microwells, which act as discrete sites for surface-enhanced Raman scattering (SERS), is reported. Development of such a novel array with discrete macroporous sites requires multiple fabrication steps. First, selective wet-chemical etching of the distal face of a coherent optical fiber bundle produces a microwell array. The microwells are then selectively filled with a macroporous structure by electroless template synthesis using self-assembled nanospheres. The fabricated arrays are structured at both the micrometer and nanometer scale on etched imaging bundles. Confocal Raman microscopy is used to detect a benzenethiol monolayer adsorbed on the macroporous gold and to map the spatial distribution of the SERS signal. The Raman enhancement factor of the modified wells is investigated and an average enhancement factor of 4×10^4 is measured. This demonstrates that such nanostructured wells can enhance the local electromagnetic field and lead to a platform of ordered SERS-active micrometer-sized spots defined by the initial shape of the etched optical fibers. Since the fabrication steps keep the initial architecture of the optical fiber bundle, such ordered SERS-active platforms fabricated onto an imaging waveguide open new applications in remote SERS imaging, plasmonic devices, and integrated electro-optical sensor arrays.

1. Introduction

The fabrication of macroporous materials with ordered 3D architectures is a very active research area of interest for various fields ranging from electrochemistry and superhydrophobicity to biosensing and nanophotonics.[1–4] The main characteristics of such porous materials in the electroanalytical domains are their high surface/volume ratio, excellent conductivity, and the interconnectivity between the pores, which makes them very attractive for miniaturized electrochemical devices.[5,6] Furthermore, the macroporous surface electrodes can be functionalized with different biomolecules to obtain biosensors.[2] In optics, these materials fabricated with various metals also exhibit unique surface plasmon properties since they can concentrate an electromagnetic field.[7,8] Macroporous materials have thus been exploited as exceptional substrates for surface-enhanced Raman scattering (SERS).[9–13] In the past decades, SERS has emerged as a new branch of the Raman technique, enabling the selective detection of various analytes at infinitesimal concentration and giving information on the structures and interactions or on the local environment at the molecular scale. The enhancement of the inherently weak Raman signal is due primarily to localized surface-plasmon resonance occurring at roughened or nanostructured noble metal surfaces.[14,15] SERS spectroscopy keeps the selectivity of Raman spectroscopy and the "fingerprint" signature of the analyte, which is directly related to the sharp vibrational spectral bands. These characteristics open up new perspectives for sensitive analysis even in complex biological environments. In this paper, we report the fabrication by template synthesis of new macroporous substrates onto the distal face of an optical fiber bundle. Confocal Raman microscopy experiments demonstrate that these arrays of macroporous microwells are 3D SERS-active platforms.

A wide variety of approaches have been developed to fabricate efficient SERS substrates. Appropriate fabrication is key to ensuring the efficient excitation of the localized surface-plasmon resonance.[11,13,16–18] Electrochemically roughened surfaces were initially exploited for SERS measurements.[19–21] Later, more sophisticated designs and shapes (e.g., nanopyramids, nanocups, nanorings, nanocrescents, etc.), enabling tuning of the surface-plasmon properties were fabricated using various techniques (e.g., electron-beam lithography, nanosphere lithography, colloidal self-assembly, etc.). For example, electrodeposition using colloidal crystals as a template produced nanovoids with a very high Raman enhancement factor.[1,9,13] More recently, multiscale engineered

[*] Prof. P. Ugo, M. Zamuner
Department of Physical Chemistry
University of Venice
Santa Marta 2137, 30123 Venice (Italy)
E-mail: ugo@unive.it
Prof. N. Sojic, M. Zamuner, D. Talaga, F. Deiss, V. Guieu, Prof. A. Kuhn
Institut des Sciences Moléculaires
UMR 5255 CNRS
Université Bordeaux 1
ENSCPB (France)
E-mail: sojic@enscpb.fr

DOI: 10.1002/adfm.200900752

SERS substrates formed by regular nanoparticle arrays have been designed with rational criteria to induce large enhancement factors.[22,23]

Optical fiber bundles are well-established tools in optics and in analytical chemistry. Such bundles comprise thousands of individually clad micrometric optical fibers (also called cores). The ordered architecture of the cores forming the bundle is maintained from the input to the output end. Therefore, an image can be carried and transmitted from one end to the other. They are flexible and small tools that allow one to perform analysis in situ. But this bundle can also be considered as a starting material that may be sculpted to induce new optical or analytical properties. Arrays of wells or of nanotips have been created, depending on the materials forming the core and the cladding of the bundle, and on the etching parameters.[24,25] Each microwell or nanotip corresponds to an optical fiber core which guides light. The microwell geometry inscribed onto the etched distal face of the optical fiber bundle has also been exploited to develop several pioneering bioanalytical applications[26,27] and successful commercial products.[28,29] The microwell arrays have been used as a matrix to immobilize living cells or beads for DNA chips, artificial olfactory systems, and multiplexed ECL immunoassays.[27,30] Pantano and co-workers functionalized the wells with chemical sensing layers.[31–34] Such a microwell represents a femtoliter-sized reaction volume with specific optical and analytical properties. These confined volumes have been used to measure the activity of single enzyme molecules and also to detect single-molecule DNA hybridization using enzymatic amplification.[35–36] It is in fact applied in an array format to detect proteins present in blood at very low concentration levels.[29] Such imaging waveguides have also been used as SERS-active substrates after controlled wet etching of the bundle.[37–41] This etching process has been recently rationalized by Stoddart and co-workers.[42] Individual optical fibers and photonic crystal fibers have also been structured at the micrometric and nanometric scale to enhance Raman signals.[43–47] Combining optical waveguides such as optical fiber bundles and SERS offers the advantages of the molecular signature of Raman spectroscopy, large enhancement factor of SERS, flexibility and compactness of optical fibers, and remote imaging possibility of the bundle format.

As mentioned, we wish to report first the fabrication of a novel high-density array of wells filled with macroporous gold. The array was fabricated on the distal face of an etched optical fiber bundle. The macroporous gold structure was created inside the microwells by exploiting the electroless deposition method. The uniform deposition of metals into colloidal arrays is challenging.[9,48] Some previous studies reported the use of gold electroless deposition to create the macroporous structure by using colloidal silica modified with thiol surface groups.[48] These were immersed in a colloidal gold solution and the gold particles attached to the thiol groups acted as catalysts in a following electroless deposition step. An easier activation technique, based on the use of a gold film coating obtained by vaporization, was recently introduced, but to deposit copper.[49] In our work, a thin gold layer sputtered on the cavity wells is used as catalyst directly for gold electroless deposition; in order to create the desired nanostructures the deposition is started from the microcavity walls. The sputtered gold acts as catalyst for the following localized electroless gold deposition. In a second part, confocal Raman microscopy was used to detect the high intensity Raman spectra of a benzenethiol monolayer adsorbed on the macroporous gold and to map the spatial distribution of the SERS-active spots.

2. Results and Discussions

The starting material is an optical fiber bundle (OFB) comprising 6 000 individually clad 3–4-μm-diameter optical fibers. The coherent structure of the OFB (global diameter: 300 μm) used in this work transmits an image through the imaging fiber with a micrometric resolution since each core acts as a pixel. Fabrication of an array with discrete macroporous SERS-active sites required multiple steps, which are depicted in Figure 1.

2.1. Fabrication and Characterization of the Etched Microwell Array

Selective wet etching (Fig. 1B) was achieved by making use of the difference in the etching rate between the high-refractive-index GeO_2-doped core and the low-refractive-index fluorine-doped cladding.[24,25,37,38,40,50] In the chosen etching conditions, GeO_2 cores dissolve at a faster rate than the cladding, thus allowing the formation of a microwell array.[24] The etching rate of the cores depends on the doping concentration and on the concentration of the acid solution. Figure 2A–C displays the surface of the imaging fiber treated for different etching times; namely 10, 30, and 60 seconds. The images indicate that the diameter of the cavities does not change significantly with the etching time whereas the well depth is proportional to etching time.[24] Since the depth is difficult to measure using scanning electron microscopy (SEM) or atomic force microscopy (AFM) in such a constrained geometry, the etched OFB was used as a template for gold deposition. The deposition was performed electrochemically using a sputtered OFB as working cathode. A gold ''negative'' image of the wells was obtained by mechanically stripping the gold deposit, which can be further imaged by SEM. Kostovski et al. used recently a similar procedure with a PDMS replica of an etched OFB for biosensing.[51] Figure 2D shows an image of the gold negative of the microcavities obtained after 60 s etching. The depth of the cavities is estimated to be ~3 μm. This evidence indicates that homo-

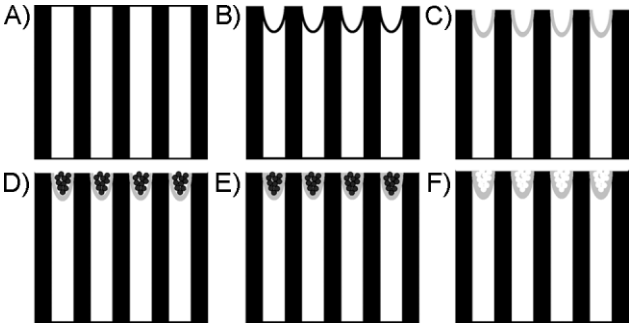

Figure 1. Schematic diagram (side view) displaying the typical process sequence (see text for details) for the fabrication of the array. Black and white represent the cladding and the cores, respectively. Gray represents the gold deposit, and the black circles are the polystyrene beads. The figure is not to scale.

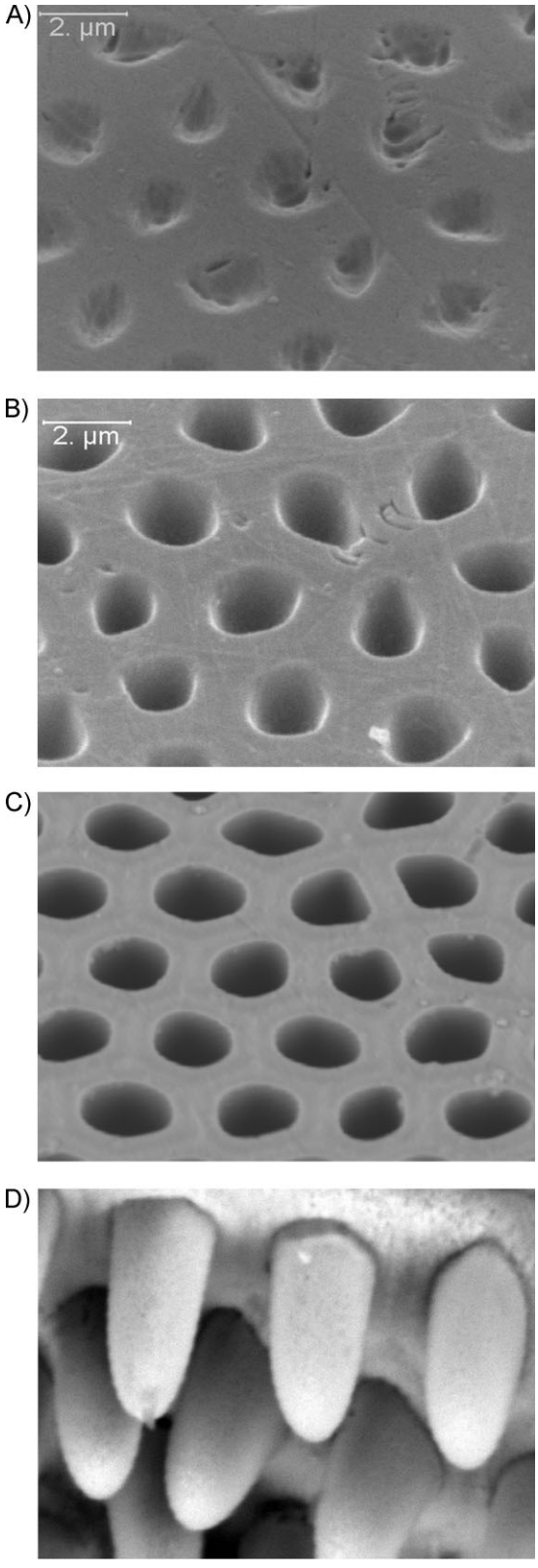

Figure 2. SEM images of the optical fiber bundles after etching times of A) 10, B) 30, and C) 60 s. D) SEM image of the gold replica of the etched and electrochemically gold-filled microwells that have been peeled off and observed from the bottom.

geneous wells are distributed in a hexagonal array format. The electroless gold procedure requires a preliminary gold deposition step to activate the surface. This was achieved by sputtering a thin (~6 nm) gold layer on the microwell surface. In order to deposit gold only in the microwells, the gold layer sputtered on the smooth flat clad was removed with a damp cotton swap (Fig. 1C). The gold surface sputtered on the walls of the wells will act as catalyst in the gold electroless deposition, which is described in Section 2.3.

2.2. Fabrication of the Colloidal Template Inside the Microwells

The formation of the 3D macroporous structures inside the microwells requires the use of close-packed arrays of monodisperse beads to act as templates in the subsequent metal deposition.[9,52] In order to obtain the assembly of the polystyrene spheres the solvent evaporation method was used. With this method the particle packing is induced by evaporation. Indeed, the liquid meniscus formed between two spheres partially immersed results in strong capillary forces. In the case of the microwells, this effect is probably combined with the packing of the beads inside the microwells by sedimentation.[53] Figure 3 displays the microbead self-assembly inside the cavities obtained by deposing 10 μL of a 2% w/w monodisperse polystyrene bead (diameter 280 nm) solution in water on the distal face of the etched OFB. It takes roughly 2 hours to achieve satisfactory self-assembled templates (Fig. 1D) which is short compared to other methods, such as the sedimentation method, which takes several days to obtain similar results. The wells are completely filled by the beads. However, the obtained bead arrangement is not perfectly ordered but more random. This is probably a consequence of the round profile of the cavities, which does not favor the achievement of ordered bead-layer stratification. This point can be addressed in future work by using a different OFB material.

2.3. Electroless Deposition Method

An electroless deposition procedure was used to fill the voids of the colloidal template inside the wells. Electroless metal deposition

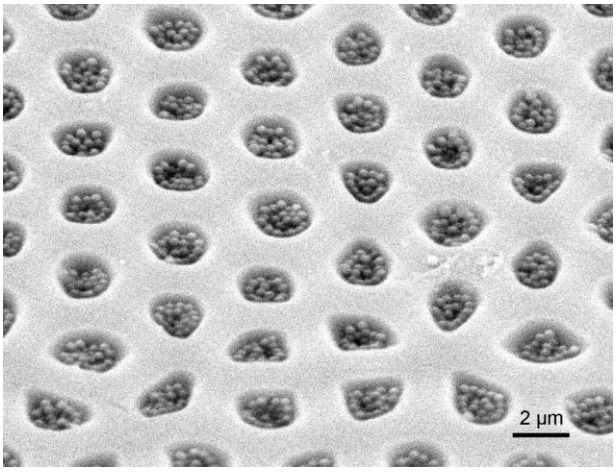

Figure 3. SEM images of the etched microwells filled with polystyrene beads (radius = 140 nm).

involves the use of a chemical reducing agent to plate a metal from solution onto a surface.[54] To avoid gold deposition outside the wells and on the cladding, the walls of the wells were sputter-coated with a thin gold layer, as previously described (Fig. 1C). This allows the following electroless deposition to take place only inside the microwells. Indeed, the thin gold layer represents excellent catalytic sites for the oxidation of formaldehyde and the concurrent reduction of gold. Once the beads were deposited inside the golden microwells to create the colloidal template, the modified OFB was dipped in a Au plating bath. Formaldehyde as the reducing agent was then added to initiate the metal growth starting at the gold-coated walls (Fig. 1E). The gold-coated wells act then as catalysts for the reduction of Au(I) by formaldehyde according to Reaction 1:[54]

$$2Au^{+} + HCHO + 3OH^{-} \rightarrow HCOO^{-} + 2H_2O + 2Au^{0} \quad (1)$$

In preliminary experiments, gold was effectively deposited inside the microwells but the cavity was not completely filled with the macroporous structure. Under these experimental conditions, the final structure corresponds to a gold layer (~500 nm) coating the walls but not completely filling the wells. The inner surface of the microcavities is very rough with nanometer sized features (data not shown). In order to increase the filling of the interstitial spaces between the colloidal template, the sample was immersed in the electroless solution for a further 1 day. The wells were filled with gold; a macroporous structure inside the cavities was visible but the dissolution of the polystyrene beads was not possible. It seems that the beads were coated by a thin gold shell that prevented the template dissolution with an organic solvent. Similar results were obtained when we deposited Sn^{2+}-sensitized beads[54] into the wells. In this case, the gold electroless deposition started from the bead surface and a gold shell was formed around them. To avoid these issues, the electroless procedure was optimized with the gold-coated wells by varying the following experimental parameters: temperature, pH, and reaction time. From the stoichiometry of Reaction 1, one can see that the pH plays an important role in the gold electroless deposition, both on the morphology and on the deposition rate.[55] Increasing pH accelerates the kinetics of Au deposition. It was important to control the electroless kinetics of the gold in this confined volume to avoid overly fast growth, which can cause a clogging of the pores as observed under some experimental conditions. Indeed, we want to fill the interstitial space between the spheres and not to create a shell around them. As seen in Figure 4, the best results were obtained at 4 °C and at pH 9.5 for 29 h. With these parameters, the beads were accessible to the organic solvent.

In order to dissolve the polystyrene beads inside the gold macroporous structure the modified bundle surface was immersed in toluene (Fig. 1F). We used SEM to characterize the morphology of the porous well array. Figure 4A shows the surface of the modified array. The great majority of the wells are filled with a macroporous gold structure with monodisperse pores. Moreover, there is almost no gold deposited during the electroless step outside the wells. A well-ordered macroporous well array is thus fabricated by this procedure. The inset of Figure 4A shows a high-magnification image and clearly reveals the pores formed after the last dissolution step. The pore diameter correlates exactly with the diameter of the polystyrene beads used to create the

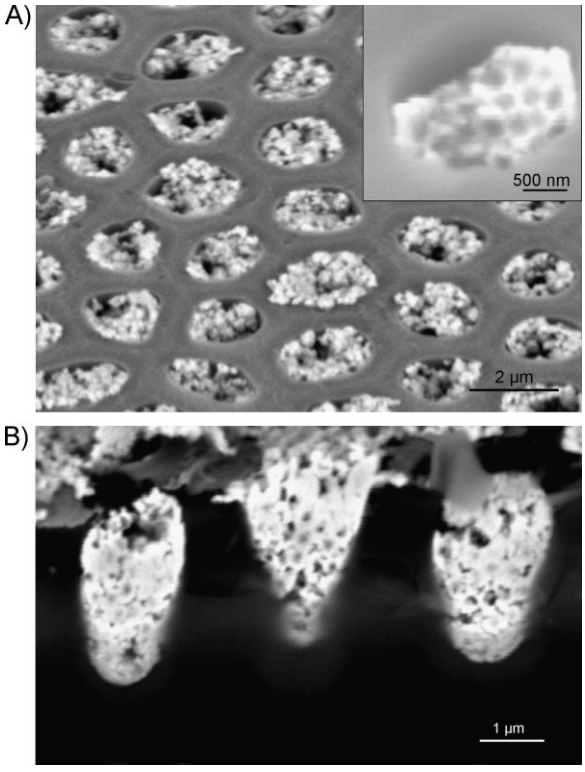

Figure 4. A) SEM image of the macroporous gold microwell array. The inset shows the pores from the top at a higher magnification. B) Cross-section view of modified microwells.

template. To image the inner part of the final wells, the array was cleaved mechanically. Figure 4B displays a cross-section view of three modified wells after this cleaving step. One can observe that pores have been formed both inside the wells and at the top surface of the array, even if the inner structure has been probably altered by the mechanical cleaving. So since the initial polystyrene beads have been dissolved inside the wells, it indicates that the organic solvent was able to diffuse inside the macroporous structure and therefore the pores are interconnected. This generates a large surface area that could be also used for electrochemical reactions in such confined volumes in an array format. It can be noted that, in principle, the gold macroporous structures could be grown by electrochemical Au deposition; however, this requires the presence of an electrical contact, for example, a sputtered gold layer extended continuously over the entire surface of the etched distal face of the OFB. As a consequence, the gold deposition would be grown not only inside the microwells (as achieved by the electroless method), but also on the flat claddings.

2.4. Raman Confocal Imaging of the Macroporous Array

We investigated the SERS effect of the multiscaled array by confocal Raman microscopy. We functionalized the array by immersing overnight the modified face of the OFB in a 10^{-2} mM benzenethiol solution in pure ethanol. The surface was then washed with ethanol to remove excess benzenethiol not bound to

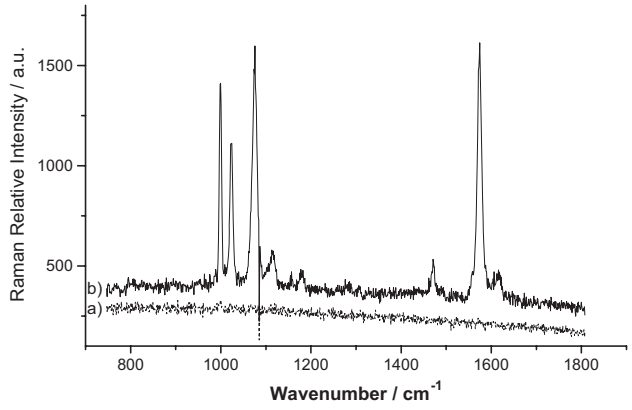

Figure 5. Typical Raman spectra of a benzenethiol monolayer adsorbed on the flat cladding surface (a) and at a gold macroporous microwell (b) using a 100×, 0.9 N.A objective. The acquisition time was set to 1 s per spectrum. Laser power: 0.2 mW; $\lambda_0 = 647$ nm.

the surface. Benzenethiol is covalently linked to the gold surface via a S–Au bond and forms a stable monolayer on the surface of the microwell array. Benzenethiol is a suitable molecule for investigating SERS since it forms stable self-assembled monolayers on gold metal surfaces and it demonstrates well-known enhanced Raman features in non-resonant conditions. Raman spectra were recorded using 647-nm laser radiation in a back-scattering geometry.

Since etched OFBs have been reported as SERS substrates,[37–41] we first checked our well array before filling it with the macroporous structure, that is, on the well array surface (Fig. 2C), which was simply sputter-coated by smooth gold and modified by the benzenethiol. The recorded spectrum (Fig. 5a) shows no characteristic feature for benzenethiol monolayer in non-resonance conditions. In other words, the simple surface of a microwell array after gold sputtering does not cause any significant Raman enhancement. This seems in contrast to previous reports in which SERS effects were observed even on microwell arrays obtained by etching the distal face of an imaging fiber. However, in these examples,[37–41] nanotips of different shapes and nanowells were created on the OFB depending on the pulling and etching parameters. The corresponding sharp features were able to create localized surface plasmon resonance and Raman enhancement.

Figure 5b is the Raman spectrum recorded on the functionalized-macroporous microwell array surface. This spectrum obtained from the benzenethiol monolayer adsorbed on the macroporous wells appears significantly enhanced as compared to the empty wells under the same experimental conditions. As mentioned in the Introduction, such a Raman enhancement induced by similar macroporous structure has been reported before by Bartlett and co-workers.[13] As no resonance Raman effect is expected when using 647-nm excitation for benzenethiol, the enhanced Raman signal observed thus strictly originates from an electromagnetic SERS effect induced by the nanostructured gold surface. In the 750–1 800-cm^{-1} spectral range, characteristic benzenethiol bands are clearly visible at 998 cm^{-1} (ν_{12}), 1 022 cm^{-1} (ν_{18a}), 1 072 cm^{-1} (ν_1), 1 111 cm^{-1} ($\nu_{6a} + \nu_{7a}$), and 1 581 cm^{-1} (ωC=C, 8a and 8b).[56] The 1 072 cm^{-1} band intensity in the SERS spectrum was significant, being characterized by a noticeable downshift from 1 092 cm^{-1} observed in solution. The intensity increase in the symmetric stretching mode (ν_1) is probably due to the specific orientation and packing of the benzenethiol monolayer on the gold surface.

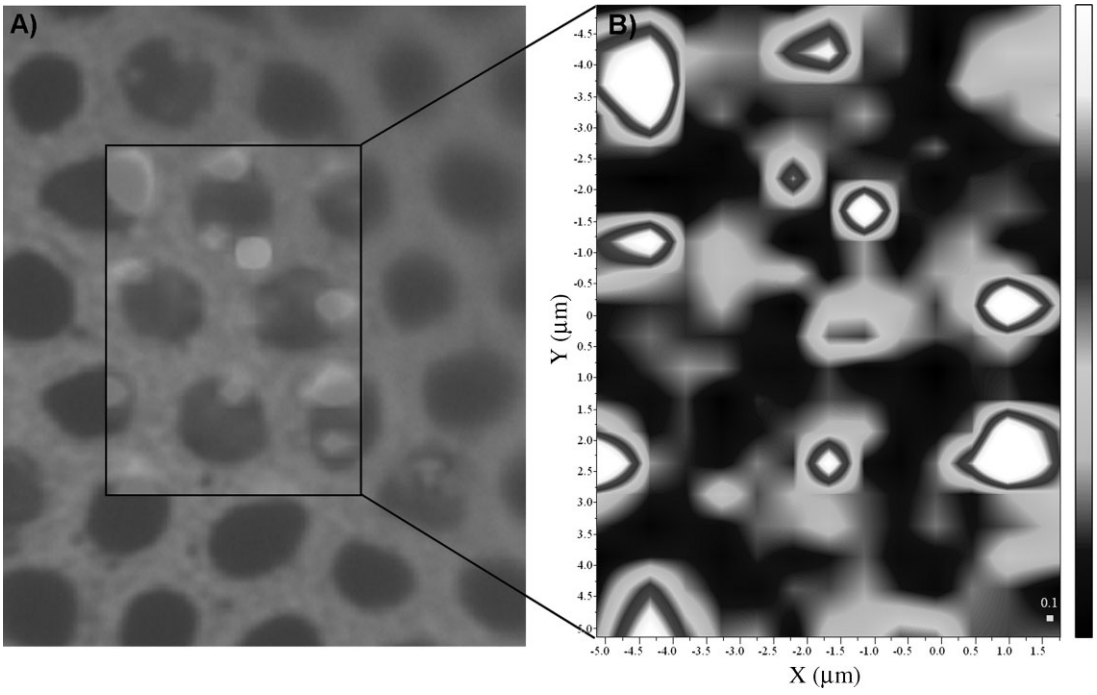

Figure 6. A) Video image of the surface array; the frame depicted corresponds to the area where Raman spectra were recorded. B) Raman images based on the υ_1 phenyl mode vibration at 1 072 cm^{-1} of the benzenethiol mapped over the macroporous microwell array. The objective is focused at the surface of the array. The stepping size was 0.5 μm. The same experimental conditions as in Figure 5 were used.

In addition to SERS spectra acquisition, confocal Raman microscopy was employed to obtain spatially resolved information in order to localize where maximum enhanced Raman spectra are observed on the SERS substrates. Mapping of the multiscaled array was performed by recording step-spectra every 500 nm with an integration time of 1 s. Figure 6A displays an optical image of the array surface focused on the hexagonal-like pattern. Figure 6b shows the Raman intensity distribution of the 1 072 cm^{-1} benzenethiol band with high intensity corresponding to the ν_1 stretching modes of the benzene ring. This image was obtained by recording spectra over lines within the (10.5×7.5) μm^2 frame depicted in Figure 6A. The most intense Raman signals reported in Figure 6b are localized for spots whose arrangement coincides with the hexagonal array of nanostructured wells. No signal is observed on the cladding (i.e., between the wells). This therefore validates the fabrication procedure of this novel multiscaled array as a SERS platform. In future works, it could be interesting to probe the contribution of each macroporous layer to the SERS enhancement and to examine the effect of the depth of the optical microwell.

To estimate the Raman enhancement effect of the nanopatterned structure inside the microwell, the Raman enhancement factor (REF) was evaluated by comparing the measured SERS intensities (I_{SERS}) with the un-enhanced Raman scattering intensities (I_{REF}) using Equation 1:[15,41,47,57]

$$\mathrm{REF} = \frac{I_{SERS}}{I_{REF}} \frac{N_{REF}}{N_{SERS}} \frac{P_{REF}}{P_{SERS}} \frac{t_{REF}}{t_{SERS}} \quad (1)$$

where N_{REF} and N_{SERS} correspond to the number of molecules illuminated by the laser in the reference solution and adsorbed on the patterned structure, respectively. The intensity denoted I is the peak intensity measured at 1 072 cm^{-1}, where the SERS effect is high. Finally P and t are respectively the laser power and the exposure time. To calculate the number of molecules adsorbed on the golden nanostructured pattern, it was assumed that the gold was deposited up to half height of the first microbead layer. Knowing that the benzenethiol molecular area is 0.22 nm^2,[40,41] and the laser spot diameter, it was possible to estimate the Raman enhancement factor: $\mathrm{REF} \approx 4 \times 10^4$. This calculated value is relatively high and comparable to the enhancement effects obtained using nanotip arrays.[40,41] However, it should be considered as a rough estimation since the precise geometry of the metallic material is not known. The SERS characterization confirmed enhancement of the Raman signal by the macroporous structure deposited inside the microwells, and thus the possibility of using this macroporous microwell array as a substrate for SERS analysis.

3. Conclusions

The fabricated arrays were structured at both micrometric and nanometric scales on the distal face of an etched optical fiber bundle. Such multiscaled substrates were developed using a combination of chemical etching, self-assembly, and deposition techniques. All these steps exploited some peculiarities of the imaging fiber: selective wet-chemical etching; self-assembly of polystyrene beads inside the wells; electroless gold deposition in the sputtered wells. We demonstrated that the enhancement of the Raman signal is localized at the modified wells. Further studies are in progress to improve the geometric order of the macroporous structure deposited inside the wells of the etched array. This should lead to a further enhancement of the SERS signal. Each SERS spot is optically wired to the corresponding core of the imaging fiber and they could be individually interrogated and imaged through it. Therefore, since the SERS array is developed on an optical fiber bundle, its intrinsic properties could be associated to perform remote SERS imaging. Our approach should allow concomitantly SERS sensing within micro-environments and direct imaging of the sample. Moreover, this array of macroporous micrometer-sized structures can be used both as optical arrays useful for SERS application and as arrays of macroporous microelectrodes. This integrated platform, combining electrochemistry and SERS measurements in such confined environments, opens up new challenging applications for remote SERS detection of bioanalytes and the development of new plasmonic devices.

4. Experimental

Materials: The OFBs were FIGH-06-300S (Fujikura), composed of 6 000 single optical cores. The silica cores were doped with GeO_2 and the cladding with fluorine. A silicone resin coated the bundle. The commercial gold electroless plating solution (Oromerse Part B, Technic Inc.) was diluted (40 times with water) prior to use. Benzenethiol (99% Sigma–Aldrich), absolute ethanol (99.9%, Sigma–Aldrich), and other grade reagents were used as received. The monodisperse polystyrene beads (diameter 280 nm) were prepared by surfactant-free emulsion polymerization of styrene initiated by potassium peroxodisulfate.

Sample Fabrication: The 300-μm diameter OFBs were polished with 5-, 1-, and 0.3-μm lapping films (Thorlabs LFG03P). The black coat protecting the fibers was removed on one face with a cotton swab wet with acetone. After polishing, the face of the OFB was dipped vertically at room temperature into 3 mL of etching solution. This solution consisted of a buffered solution composed of ammonium fluoride 40% (in water from 99%), hydrofluoric acid 48 wt% (in water), and hydrochloric acid 36.8% composed by 5/1/11 of NH_4F/HF/HCl. The reaction was quickly quenched in deionized water. CAUTION: Hydrofluoric acid is extremely corrosive and toxic. Safety procedures must be followed accordingly. Gold-sputtering was conducted with an Emitech K550X sputter-coater.

Electroless Gold Deposition: Once the beads were deposited inside the golden microwell to create the colloidal template, the modified bundle was immersed into 1 mL of Au plating bath composed of 7.9×10^{-3} M in $Na_3Au(SO_3)_2$, and 0.127 M in Na_2SO_3. 20 μL of formaldehyde 0.625 M was then added to the plating bath. The pH of the plating bath (initially around 10) was changed by adding 0.025 M $NaHCO_3$ and by dropwise addition of NaOH (pH 12 or 14) or H_2SO_4 (pH 9).

SERS Measurements: The SERS analysis was performed by recording step spectra every 500 nm with an integration time of 1 s, spot size 1 μm. Raman spectra were recorded on a Labram HR (Horiba-Jobin-Yvon) spectrometer using a 647-nm Ar–Kr laser at a power of 0.2 mW, irradiating the surface of the OFB. The microscope objective used for the confocal microscope was purchased from Olympus (MPlan 100×, N.A. 0.9). The images were detected by a Symphony CCD camera.

Acknowledgements

The authors thank the Agence Nationale pour la Recherche (Programme en Nanosciences et Nanotechnologies ANR-05-NANO-048), the CNRS (Chemistry department), the Région Aquitaine and MIUR (Rome) for

financial support. M. Z. wish to thank the Ministère des Affaires Etrangères et Européennes for a ''Bourse d'excellence Eiffel'' fellowship.

Received: April 30, 2009
Published online: August 19, 2009

[1] S. Cintra, M. E. Abdelsalam, P. N. Bartlett, J. J. Baumberg, T. A. Kelf, Y. Sugawara, A. E. Russell, *Faraday Discuss.* **2006**, *132*, 191.
[2] A. Walcarius, A. Kuhn, *TrAC Trends Anal. Chem.* **2008**, *27*, 593.
[3] Z. Chen, T. Gang, Y. Wang, X. Chen, C. Guan, J. Zhang, Z. Sun, K. Zhang, B. Zhao, B. Yang, *Colloids Surf. A* **2006**, *277*, 37.
[4] W. Huang, M. Wang, J. Zheng, Z. Li, *J. Phys. Chem. C* **2009**, *113*, 1800.
[5] R. Szamocki, S. Reculusa, S. Ravaine, P. N. Bartlett, A. Kuhn, R. Hempelmann, *Angew. Chem. Int. Ed.* **2006**, *45*, 1317.
[6] R. Szamocki, A. Velichko, C. Holzapfel, F. Mucklich, S. Ravaine, P. Garrigue, N. Sojic, R. Hempelmann, A. Kuhn, *Anal. Chem.* **2007**, *79*, 533.
[7] T. V. Teperik, F. J. Garcia de Abajo, A. G. Borisov, M. Abdelsalam, P. N. Bartlett, Y. Sugawara, J. J. Baumberg, *Nat. Photon.* **2008**, *2*, 299.
[8] S. Coyle, M. C. Netti, J. J. Baumberg, M. A. Ghanem, P. R. Birkin, P. N. Bartlett, D. M. Whittaker, *Phys. Rev. Lett.* **2001**, *87*, 176801.
[9] P. N. Bartlett, J. J. Baumberg, S. Coyle, M. E. Abdelsalam, *Faraday Discuss.* **2004**, *125*, 117.
[10] L. Lu, A. Eychmüller, A. Kobayashi, Y. Hirano, K. Yoshida, Y. Kikkawa, K. Tawa, Y. Ozaki, *Langmuir* **2006**, *22*, 2605.
[11] G. A. Baker, D. S. Moore, *Anal. Bioanal. Chem.* **2005**, *382*, 1751.
[12] P. M. Tessier, O. D. Velev, A. T. Kalambur, J. F. Rabolt, A. M. Lenhoff, E. W. Kaler, *J. Am. Chem. Soc.* **2000**, *122*, 9554.
[13] J. J. Baumberg, T. A. Kelf, Y. Sugawara, S. Cintra, M. E. Abdelsalam, P. N. Bartlett, A. E. Russell, *Nano Lett.* **2005**, *5*, 2262.
[14] K. A. Willets, R. P. Van Duyne, *Annu. Rev. Phys. Chem.* **2006**, *58*, 267.
[15] E. C. Le Ru, E. Blackie, M. Meyer, P. G. Etchegoin, *J. Phys. Chem. C* **2007**, *111*, 13794.
[16] S. Lal, N. K. Grady, J. Kundu, C. S. Levin, J. B. Lassiter, N. J. Halas, *Chem. Soc. Rev.* **2008**, *37*, 898.
[17] R. J. C. Brown, M. J. T. Milton, *J. Raman Spectrosc.* **2008**, *39*, 1313.
[18] T. Vo-Dinh, *TrAC Trends Anal. Chem.* **1998**, *17*, 557.
[19] M. Fleischmann, P. J. Hendra, A. J. McQuillan, *Chem. Phys. Lett.* **1974**, *26*, 163.
[20] D. L. Jeanmaire, R. P. Van Duyne, *J. Electroanal. Chem.* **1977**, *84*, 1.
[21] C. L. Haynes, C. R. Yonzon, X. Zhang, R. P. Van Duyne, *J. Raman Spectrosc.* **2005**, *36*, 471.
[22] A. Gopinath, S. V. Boriskina, B. M. Reinhard, L. Dal Negro, *Opt. Express* **2009**, *17*, 3741.
[23] B. Yan, A. Thubagere, W. R. Premasiri, L. D. Ziegler, L. Dal Negro, B. R. M. Reinhard, *ACS Nano* **2009**, *3*, 1190.
[24] P. Pantano, D. R. Walt, *Chem. Mater.* **1996**, *8*, 2832.
[25] P. Pantano, D. R. Walt, *Rev. Sci. Instrum.* **1997**, *68*, 1357.
[26] D. R. Walt, *Curr. Opin. Chem. Biol.* **2003**, *6*, 689.
[27] C. N. LaFratta, D. R. Walt, *Chem. Rev.* **2008**, *108*, 614.
[28] Illumina, Inc., www.illumina.com (accessed July 2009).
[29] Quanterix, Inc., www.quanterix.com (accessed July 2009).
[30] F. Deiss, C. N. LaFratta, M. Symer, T. M. Blicharz, N. Sojic, D. R. Walt, *J. Am. Chem. Soc.* **2009**, *131*, 6088.
[31] D. D. Bernhard, S. Mall, P. Pantano, *Anal. Chem.* **2001**, *73*, 2484.
[32] P. Pantano, C. C. Meek, J. Wang, D. H. Coutinho, K. J. Balkus, *Lab Chip* **2003**, *3*, 132.
[33] C. C. Meek, P. Pantano, *Lab Chip* **2001**, *1*, 158.
[34] S.-F. Chin, P. Pantano, *Microchem. J.* **2006**, *84*, 1.
[35] D. M. Rissin, D. R. Walt, *Nano Lett.* **2006**, *6*, 520.
[36] H. H. Gorris, D. M. Rissin, D. R. Walt, *Proc. Natl. Acad. Sci. USA* **2007**, *104*, 17680.
[37] D. J. White, P. R. Stoddart, *Opt. Lett.* **2005**, *30*, 598.
[38] D. J. White, A. P. Mazzolini, P. R. Stoddart, *J. Raman Spectrosc.* **2007**, *38*, 377.
[39] M. E. Hankus, H. Li, G. J. Gibson, B. M. Cullum, *Anal. Chem.* **2006**, *78*, 7535.
[40] V. Guieu, F. Lagugné-Labarthet, L. Servant, D. Talaga, N. Sojic, *Small* **2008**, *4*, 96.
[41] V. Guieu, D. Talaga, L. Servant, N. Sojic, F. Lagugne-Labarthet, *J. Phys. Chem. C* **2009**, *113*, 874.
[42] D. J. White, A. P. Mazzolini, P. R. Stoddart, *Photon. Nanostruct. Fund. Appl.* **2008**, *6*, 167.
[43] A. Amezcua-Correa, J. Yang, C. E. Finlayson, A. C. Peacock, J. R. Hayes, P. J. A. Sazio, J. J. Baumberg, S. M. Howdle, *Adv. Funct. Mater.* **2007**, *17*, 2024.
[44] C. P. Anna, A.-C. Adrian, Y. Jixin, J. A. S. Pier, M. H. Steven, *Appl. Phys. Lett.* **2008**, *92*, 141113.
[45] H. Yan, C. Gu, C. Yang, J. Liu, G. Jin, J. Zhang, L. Hou, Y. Yao, *Appl. Phys. Lett.* **2006**, *89*, 204101.
[46] Y. Zhang, C. Shi, C. Gu, L. Seballos, J. Z. Zhang, *Appl. Phys. Lett.* **2007**, *90*, 193504.
[47] E. J. Smythe, M. D. Dickey, J. Bao, G. M. Whitesides, F. Capasso, *Nano Lett.* **2009**, *9*, 1132.
[48] P. Jiang, J. Cizeron, J. F. Bertone, V. L. Colvin, *J. Am. Chem. Soc.* **1999**, *121*, 7957.
[49] H. L. Cong, W. X. Cao, *Adv. Funct. Mater.* **2005**, *15*, 1821.
[50] A. Chovin, P. Garrigue, I. Manek-Hönninger, N. Sojic, *Nano Lett.* **2004**, *4*, 1965.
[51] G. Kostovski, D. J. White, A. Mitchell, M. W. Austin, P. R. Stoddart, *Biosens. Bioelectron.* **2009**, *24*, 1531.
[52] M. C. Netti, S. Coyle, J. J. Baumberg, M. A. Ghanem, P. R. Birkin, P. N. Bartlett, D. M. Whittaker, *Adv. Mater.* **2001**, *13*, 1368.
[53] E. J. Tull, P. N. Bartlett, K. R. Ryan, *Langmuir* **2007**, *23*, 7859.
[54] V. P. Menon, C. R. Martin, *Anal. Chem.* **1995**, *67*, 1920.
[55] M. De Leo, F. C. Pereira, L. M. Moretto, P. Scopece, S. Polizzi, P. Ugo, *Chem. Mater.* **2007**, *19*, 5955.
[56] A. D. McFarland, M. A. Young, J. A. Dieringer, R. P. Van Duyne, *J. Phys. Chem. B* **2005**, *109*, 11279.
[57] W. B. Cai, B. Ren, X. Q. Li, C. X. She, F. M. Liu, X. W. Cai, Z. Q. Tian, *Surf. Sci.* **1998**, *406*, 9.